

12. STABLE ISOTOPE RECORD OF THE LAST 500 K.Y. AT SITE 1087 (SOUTHERN CAPE BASIN)¹

C. Pierre,² J.F. Saliege,² M.J. Urrutiaguer,² and J. Giraudeau³

ABSTRACT

High-resolution planktonic and benthic stable isotope records from Ocean Drilling Program Site 1087 off southeast Africa provide the basis for a detailed study of glacial-interglacial (G-IG) cycles during the last 500 k.y. This site is located in the Southern Cape Basin at the boundary of the coastal upwelling of Benguela and close to the gateway between the South Atlantic and the Indian Oceans. It therefore monitors variations of the hydrological fronts associated with the upwelling system and the Atlantic-Indian Ocean interconnections, in relation to global climate change. The coldest period of the last 500 k.y. corresponds to marine isotope Stage (MIS) 12, when surface water temperature was 4°C lower than during the last glacial maximum (LGM) as recorded by the surface-dwelling foraminifer *Globigerinoides ruber*. The warmest periods occurred during MISs 5 and 11, a situation slightly different to that observed at Site 704, which is close to the Polar Front Zone, where there is no significant difference between the interglacial stages for the past 450 k.y., except the long period of warmth during MIS 11.

The planktonic and benthic carbon isotope records do not follow the G-IG cycles but show large oscillations related to major changes in the productivity regime. The largest positive $\delta^{13}\text{C}$ excursion between 260 and 425 ka coincides with the global mid-Brunhes event of carbonate productivity. The oxygen and carbon isotopic gradients between surface and deep waters display long-term changes superimposed on rapid and high-frequency fluctuations that do not follow the regular G-IG pattern; these gradients indicate modifications of the temperature, salinity, and productivity gradients due to changes in the thermocline depth,

¹Pierre, C., Saliege, J.F., Urrutiaguer, M.J., and Giraudeau, J., 2001. Stable isotope record of the last 500 k.y. at Site 1087 (Southern Cape Basin). In Wefer, G., Berger, W.H., and Richter, C. (Eds.), *Proc. ODP, Sci. Results*, 175, 1–22 [Online]. Available from World Wide Web: <http://www-odp.tamu.edu/publications/175_SR/VOLUME/CHAPTERS/SR175_12.PDF>. [Cited YYYY-MM-DD]

²Université Pierre et Marie Curie, Laboratoire d'Oceanographie Dynamique et de Climatologie, 4 Place Jussieu, 75252 Paris Cedex 05, France. Correspondence author:

cat@odyc.jussieu.fr

³Université de Bordeaux I, DGO, avenue des Facultés, 33405 Talence, France.

the position of the hydrological fronts, and the strength of the Benguela Current.

INTRODUCTION

The main objectives of Ocean Drilling Program (ODP) Leg 175, in which the participants drilled along the west coast of southern Africa, were to reconstruct the past history of the Benguela Current, which is presently associated with a system of very active upwelling cells located off shore of Angola, Namibia, and south Africa. High productivity levels ($>180 \text{ g C/m}^2/\text{yr}$) characterize the present system, which is considered to be a major zone for carbon export and thus probably exerts a strong control on the global carbon budget.

Previous studies in the region have shown that the relative positions of the oceanic fronts (the Angola-Benguela Front, located presently at $\sim 17^\circ\text{S}$; the Subtropical Convergence [STC], located presently at $\sim 38^\circ\text{S}$; and the Polar Front Zone located presently $\sim 50^\circ\text{S}$) moved farther north by a few degrees of latitude during glacial periods (Morley and Hays, 1979; Jansen et al., 1986). The northward shift of the STC was also responsible for the transfer of thermocline waters from the southwest Indian Ocean to the southeast Atlantic Ocean (Winter and Martin, 1990; Wefer et al., 1996). During glacial periods, surface productivities were much higher than during interglacials because of the strengthened trade-wind stress; at depth, the general consensus is that the glacial North Atlantic Deep Water (NADW) flux was weakened and brought nutrient-rich ^{13}C -depleted waters, whereas the Antarctic Intermediate Water (AAIW) flux was relatively strong and brought nutrient-poor ^{13}C -rich waters, compared to the interglacial situations (Sarnthein and Tiedemann, 1990; Howard and Prell, 1994).

The recovery of continuous Neogene sedimentary sequences during Leg 175 makes it possible for the first time to obtain the complete paleoceanographic record of the Angola-Benguela Current System for the last 15 m.y. The present study examines the stable isotope record of planktonic and benthic foraminifers of the last 500 k.y. at Site 1087, which is in the Southern Cape Basin. Our main objectives are to

1. Establish the precise chronological framework with the oxygen isotope stratigraphy,
2. Estimate the fluctuations of paleoproductivity from the carbon isotopic compositions of planktonic foraminifers and from the surface-to-bottom $\delta^{13}\text{C}$ gradient, and
3. Measure the isotopic gradients between different planktonic species in order to deduce temperature and productivity gradients in surface waters.

SITE 1087

Hole 1087A ($31^\circ 27.8813'\text{S}$, $15^\circ 18.6541'\text{E}$) was drilled in 1371.6-m-deep water and is bathed by the AAIW, a water mass that originates in the Polar Front Zone of the Southern Ocean. This hole penetrated 255.2 meters below the seafloor (mbsf) of sediments that were continuously drilled down to the upper Miocene. The upper 45 m of the sedimentary sequence consists of nannofossil ooze with varying abundances of clay and foraminifers, which are intercalated with sandy nannofossil for-

minifer ooze interpreted as turbidites (Shipboard Scientific Party, 1998). The average sedimentation rate in this interval is 3 cm/k.y., which is one of the lowest measured in the Benguela Current System when compared to the rates measured in the Angola Basin (up to 60 cm/k.y.) and in the Lüderitz cell (15 cm/k.y.).

METHODS

For the present study, samples have been taken each 5 cm in the upper 13 m (Samples 175-1087A-1H-1, 0–3 cm, to 2H-4, 30–32 cm) to obtain a time resolution of ~2 k.y. in the stable isotope records. A break of 40 cm occurs between Cores 1H and 2H (from Samples 175-1087A-1H-6, 51–53 cm, and 2H-1, 20–22 cm). Each sample was disintegrated in distilled water and washed on a 63- μm sieve, cleaned in an ultrasonic bath to remove fine particles, filtered, and dried. The foraminifers were then selected from the >250- μm size fraction. An average number of 10 to 12 individuals of each species was picked to obtain the weight of 200 to 250 μg that is necessary for stable isotope analyses. Stable isotope analyses were performed on the three planktonic foraminifer species *Globigerina bulloides*, *Globigerinoides ruber*, and *Globorotalia inflata* and on the benthic foraminifer species *Cibicides wuellerstorfi*.

CO_2 gas is extracted from the carbonate of the foraminifers at 90°C with dehydrated phosphoric acid on the automatic device, coupled with a triple collector Optima-Isogas mass spectrometer. The analytical precision is 0.01‰. With each 12 samples, two reference carbonates are included, giving a reproducibility of measurements made on this reference of $\pm 0.02\text{\textperthousand}$ for both $\delta^{18}\text{O}$ and $\delta^{13}\text{C}$ values. Standard deviations of three to four separated analyses of the same foraminiferal species calculated from a series of 50 samples are $\pm 0.1\text{\textperthousand}$ for $\delta^{18}\text{O}$ and $\delta^{13}\text{C}$.

All analytical data from Hole 1087A are listed in Table T1.

RESULTS

Oxygen Isotope Record

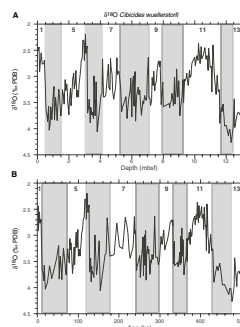
The oxygen isotope stratigraphy at Hole 1087A is based on the continuous record of *C. wuellerstorfi*, allowing the identification of MISs 1 through 13, which spans the last 500 k.y. The timescale calibration of the isotopic stages corresponds to the orbitally derived scales of Imbrie et al., (1984), Martinson et al. (1987), and Bassinot et al. (1994). The age-control points are listed in Table T2. Linear interpolation was applied between adjacent age control-points, assuming a constant sedimentation rate within the time interval. The average sedimentation rate is estimated at 2.7 cm/k.y. for the entire 13-m interval. In fact, sedimentation rates are irregular, with higher rates (3–4 cm/k.y.) during MISs 1, 2, 4, 5, 8, 10, 11, 13 and lower rates (1–1.9 cm/k.y.) during MISs 3, 7, 9, and 12.

The $\delta^{18}\text{O}$ record of *Cibicides* is given both as a function of depth (Fig. F1A) and of age (Fig. F1B). The lowest $\delta^{18}\text{O}$ values are measured during isotopic Event 5.5 (2.19‰) and MIS 11 (2.37‰), which characterize the warmest periods. The highest $\delta^{18}\text{O}$ values (4.27‰) are measured during MIS 12, which marks the coldest stage. At Site 704, which is near the Polar Front Zone in the South Atlantic (i.e., in the source area of AAIW), the coldest stage is also MIS 12, but there is no significant differ-

T1. Sample identification, depth, age, and isotopic compositions of foraminifers, Hole 1087A, p. 18.

T2. Age-control points used for the age extrapolation, Hole 1087A, p. 22.

F1. The $\delta^{18}\text{O}$ record of *C. wuellerstorfi* as functions of depth and age, Hole 1075A, p. 12.



ence between the interglacial stages for the last 450 k.y. except the long warm period during MIS 11 (Hodell, 1993; Hodell et al., 2000). If one assumes that the G-IG salinity changes were negligible in the source area of AAIW and subtracts 1.6‰ and 1.2‰ for the maximum global ice effect during Terminations V and II, respectively (McManus et al., 1999), the maximum difference of $\delta^{18}\text{O}$ values between MIS 12 and 11 and MIS 6 and 5 will equal 0.3‰ and 0.6‰, which correspond to a maximum temperature change of $\sim 1.5^\circ$ and 2.5°C in deep waters (using an ^{18}O fractionation of $-0.22\text{‰}/^\circ\text{C}$). Otherwise, this G-IG temperature variation would be less if part of the $\delta^{18}\text{O}$ variation is caused by increased freshwater dilution during interglacials. The difference of $\delta^{18}\text{O}$ values between the LGM and the Holocene is 1.6‰, indicating that during Termination I the temperature increase was $<2^\circ\text{C}$ in the deep waters at Site 1087.

The $\delta^{18}\text{O}$ records of the three species of planktonic foraminifers display similar variations, although the amplitudes of the difference between glacial and interglacial values ($\delta^{18}\text{O}$ G-IG) differ for each species (Fig. F2). For the last four G-IG cycles, the $\delta^{18}\text{O}$ G-IG amplitude decreases from 2.1‰ in *G. bulloides* to 1.5‰ in *G. inflata* and to 1.2‰ in *G. ruber*. A comparison of the *G. bulloides* and *G. inflata* records shows in fact that the glacial values are very close for the two species, whereas the low interglacial values are much lower for *G. bulloides* than for *G. inflata*; this indicates that the temperature change in surface waters occurred mostly during interglacial stages.

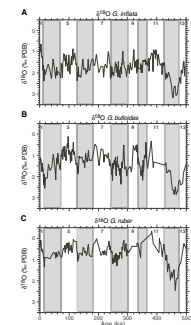
As was the case for the benthic foraminifers, the highest $\delta^{18}\text{O}$ values of the planktonic foraminifers are found during MIS 12, which corresponds to the coldest stage of the last 500 k.y. (Fig. F2). The difference in $\delta^{18}\text{O}$ values between LGM and MIS 12 ranges from 1.2‰ (*G. ruber*) to 0.4‰ (*G. bulloides*), with *G. inflata* showing an intermediate value of 0.7‰. Subtracting the global ice effect difference of 0.4‰ between LGM and MIS 12 (McManus et al., 1999) translates into an MIS 12 cooling of surface waters compared to the LGM situation of $\sim 4^\circ$ and 1.5°C , as recorded by *G. ruber* and *G. inflata*, respectively.

Carbon Isotope Record

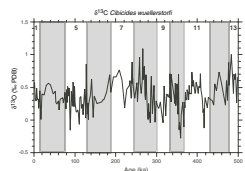
The $\delta^{13}\text{C}$ record of *C. wuellerstorfi* shows a pattern different from the G-IG cycles but linked to large oscillations much higher than the 100-k.y. eccentricity period (Fig. F3). Two intervals of lower $\delta^{13}\text{C}$ values occur between 20–160 ka and 300–420 ka and are separated by an interval of higher $\delta^{13}\text{C}$ values during the period 160–300 ka. If the $\delta^{13}\text{C}$ values of benthic foraminifers are considered to be a proxy of ventilation and nutrient concentration at depth, the AAIW was well ventilated and nutrient poor prior to 420 ka and from 160 to 300 ka, whereas it was less ventilated and nutrient rich during both 20–160 ka and 300–420 ka intervals. Furthermore, $\delta^{13}\text{C}$ values tend to decrease at the IG-G transitions, a pattern particularly well expressed at the MIS 13/12, MIS 11/10, and MIS 7/6 transitions. This $\delta^{13}\text{C}$ decrease suggests that inputs of nutrients occurred during the beginning of cool conditions at the IG-G transitions and that the migration toward the equator of the Polar Front Zone was associated with a relatively lower rate of AAIW ventilation.

Similarly the planktonic foraminiferal $\delta^{13}\text{C}$ records do not display clear evidence of G-IG cyclicity (Fig. F4). Common to the three planktonic taxa is a large positive $\delta^{13}\text{C}$ oscillation spanning the time interval 260–425 ka; this increase is the highest (2.1‰) for *G. bulloides*, interme-

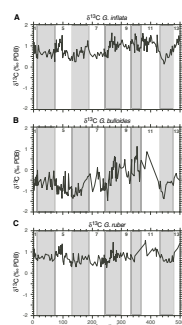
F2. The $\delta^{18}\text{O}$ record of planktonic foraminifers as a function of age, Hole 1075A, p. 13.



F3. The $\delta^{13}\text{C}$ record of benthic foraminifers as a function of age in Hole 1075A, p. 14.



F4. The $\delta^{13}\text{C}$ record of planktonic foraminifers as a function of age, Hole 1075A, p. 15.



diate ($1.2\text{\textperthousand}$) for *G. inflata*, and the lowest ($0.8\text{\textperthousand}$) for *G. ruber*. In terms of productivity levels, this positive $\delta^{13}\text{C}$ excursion identifies a highly productive period that coincides with the global mid-Brunhes event (Jansen et al., 1986) known for its very high level of pelagic carbonate production during MISs 7, 9, and 11 (Hodell, 1993). A shorter period of ^{13}C enrichment between 80 and 100 ka also suggests high productivity levels during the late MIS 5.

DISCUSSION

The differences observed in the amplitude of the planktonic and benthic $\delta^{18}\text{O}$ and $\delta^{13}\text{C}$ variations indicate that temperature, salinity, and productivity changes occurred in the surface water and deep water masses in relation to past climatic changes. The salinity variations that are related to the global ice effect are similarly recorded by the $\delta^{18}\text{O}$ values of planktonic and benthic foraminifers. The $\delta^{18}\text{O}$ gradients between foraminiferal species are thus affected only by the vertical thermal gradients and by local salinity variations at the ocean surface due to differences in the precipitation-evaporation balance.

The export of organic carbon from the photic zone extracts preferentially ^{12}C from the dissolved inorganic carbon reservoir, which becomes richer in ^{13}C ; there is thus a direct relationship between high $\delta^{13}\text{C}$ values and high rates of biological pumping in surface waters. However, inputs of deep nutrients by upwelling introduce ^{13}C -depleted CO_2 in the surface waters, which is characteristic of eutrophic conditions and causes the decrease of the surface-subsurface $\delta^{13}\text{C}$ gradient. Intermediate between oligotrophic and eutrophic conditions, mesotrophic situations exhibit high surface-subsurface $\delta^{13}\text{C}$ gradients due to the combination of lateral advection of deep nutrients and high surface productivity levels (Pierre et al., 1994). At depth, the contribution of CO_2 derived from organic matter oxidation causes a decrease of the $\delta^{13}\text{C}$ values of deep waters. During glacial times, high $\delta^{13}\text{C}$ gradients between planktonic and benthic foraminifers indicative of high productivity were generally coeval with low atmospheric CO_2 concentrations in the air trapped in antarctic ice, which was interpreted by Berger et al. (1989) as an argument on the link between the biological pump and the global concentration of atmospheric CO_2 . Recently, Broecker and Henderson (1998) have proposed that the ocean productivity changes are global and related to the oceanic nitrogen cycle, which is controlled by dust flux. In this scenario, increasing nitrogen fixation during glacial times would cause the increase of CO_2 uptake in surface waters and the drawdown of atmospheric CO_2 concentrations.

The estimation of the oxygen and carbon isotopic gradients between foraminiferal species living at different depths or at different seasons may help to reconstruct changes in surface water hydrography. Giraudeau (1993) and Giraudeau and Rogers (1994) provided information on the spatial distribution of planktonic foraminiferal species in the Benguela upwelling system. Their studies showed that planktonic assemblages are distributed according to the various surface water masses and associated hydrological fronts induced by the upwelling process. Among the three planktonic species that were used in the present stable isotope study, *G. ruber* is considered to be characteristic of warm surface waters; the subpolar species *G. bulloides* dominates the planktonic assemblages of cool, nutrient-rich, newly upwelled waters, whereas the

deep-dwelling species *G. inflata* is associated with offshore oligotrophic waters.

In the following discussion, the surface-to-deep isotopic gradients $\Delta^{18}\text{O}$ and $\Delta^{13}\text{C}$ are given by the difference between the $\delta^{18}\text{O}$ and $\delta^{13}\text{C}$ values of *G. inflata* and *Cibicides*. The isotopic gradients between *G. inflata* and *G. ruber* are used as a tracer of the seasonal or vertical (depth of the thermocline) temperature gradient in the surface mixed layer, whereas the isotopic gradients between *G. inflata* and *G. bulloides* are used as an index of the variable contributions of oligotrophic offshore waters and upwelled eutrophic waters at the site location.

Oxygen Isotopic Gradient

Surface–Deep Water Gradient

The $\Delta^{18}\text{O}$ *G. inflata*–*Cibicides* record displays large oscillations that roughly follow the G-IG cyclicity (Fig. F5A). Second-order, rapid, high-amplitude fluctuations of $\Delta^{18}\text{O}$ around the present-day gradient ($\Delta^{18}\text{O}$ values enriched by up to 1.0‰ or depleted by up to 0.8‰) are indicative of the surface-to-bottom temperature and salinity gradients. High $\Delta^{18}\text{O}$ values are interpreted as either decreasing surface-to-bottom temperature gradients or increasing surface-to-bottom salinity gradients.

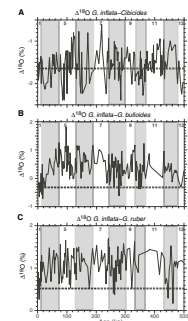
The largest oscillations of $\Delta^{18}\text{O}$ with amplitudes up to 1.8‰ occur between 80 and 280 ka, a period that comprises MISs 5 to 8. Such high amplitudes cannot be attributed to changes of up to 8°C in the surface-to-bottom temperature gradient because such temperature changes would be extreme. We therefore consider that surface waters were also affected by important salinity variations. A comparison of the isotopic data with the planktonic foraminiferal distribution at Hole 1087A (Giraudeau et al., Chap. 7, this volume) shows that some peaks of high $\Delta^{18}\text{O}$ values (terminations I and II, MISs 11 and 12) are in phase with the peaks of abundance of *G. menardii*, both proxies indicating maximum penetration of salty $\Delta^{18}\text{O}$ -rich Indian Ocean thermocline waters. Other peaks of high $\Delta^{18}\text{O}$ values (MISs 4, 5, 6, 7, 8, and 12) coincide with the maximum abundances of *G. bulloides*, which suggests the presence of cold, upwelled surface water. Low $\Delta^{18}\text{O}$ values generally occur during cold events of glacial and interglacial stages; if these isotopic gradients are interpreted in terms of the surface-to-bottom temperature gradient, the cooling of surface waters had to be less than that of deep waters.

Surface Water Gradients

The amplitude of $\delta^{18}\text{O}$ variations through time is greatest for *G. bulloides* and least for *G. ruber*, except for MIS 12. This is reflected by the planktonic $\Delta^{18}\text{O}$ variations; for example, the amplitude for *G. inflata*–*G. bulloides* is twice that of *G. inflata*–*G. ruber* (Fig. F5B, F5C). MIS 11 is poorly constrained due to the scarcity of *G. bulloides* and *G. ruber* during this time interval.

The $\Delta^{18}\text{O}$ *G. inflata*–*G. bulloides* is generally much higher than during the Holocene, except for a few rapid events during MIS 2, 8, and 10 that reach the Holocene level (Fig. F5B). The overall high $\Delta^{18}\text{O}$ values, particularly during isotopic events 5.3 and 9.3, are caused by an increase in $\delta^{18}\text{O}$ values of *G. inflata* and a decrease in $\delta^{18}\text{O}$ values of *G. bulloides*. Conversely, the $\Delta^{18}\text{O}$ decreases, such as those observed at the MIS transitions 11/10, 7/6, 5/4, and 4/3, correspond to rather constant $\delta^{18}\text{O}$ val-

F5. The $\Delta^{18}\text{O}$ gradient between *G. inflata* and *Cibicides*, *G. bulloides*, and *G. ruber* as a function of age, Hole 1087A, p. 16.



ues of *G. inflata* and to increasing $\delta^{18}\text{O}$ values of *G. bulloides*. These isotopic variations integrate the variations of a multicomponent system where the seaward extension of the upwelled waters relative to the offshore oligotrophic waters is modulated by the cooling intensity in the upwelling cell and by the strength of the Benguela Current.

The $\Delta^{18}\text{O}$ *G. inflata*-*G. ruber* and $\Delta^{18}\text{O}$ *G. inflata*-*G. bulloides* records display very similar vertical patterns (Fig. F5C). They show no difference in their amplitude during G-IG cycles; however, the highest $\Delta^{18}\text{O}$ values occur during the warm substages reflecting periods of higher temperature contrast in the surface waters. The onset of deglaciations displays a typical evolution with a sharp increase followed by a sharp decrease of $\Delta^{18}\text{O}$ values; this can be interpreted either as a succession of deepening and shoaling of the thermocline or as abrupt changes from high to low seasonal contrast. Similar observations were made by Wefer et al. (1996) in the Benguela Current System, and these authors emphasized the difficulty of interpreting this proxy in terms of seasonal contrast or thermocline depth. In any case, this evolution would mean that the Benguela Current was temporarily reduced at the end of glacial stages and then reinforced at the beginning of interglacial stages.

Carbon Isotopic Gradient

Surface-Deep Water Gradient

The $\Delta^{13}\text{C}$ *G. inflata*-*Cibicides* values are subjected both to sharp short-term and long-term oscillations, with a maximum amplitude of $1.7\text{\textperthousand}$, that are not related to the G-IG cycles (Fig. F6A). The $\Delta^{13}\text{C}$ variations thus are quite different from the pattern described by Berger et al. (1989). We assume that at Site 1087, latitudinal and meridional migrations of hydrological fronts dominated the surface water productivity.

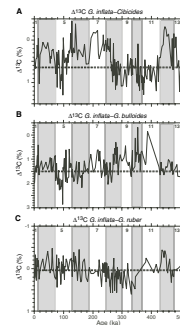
The short-term periods of low $\Delta^{13}\text{C}$ values, which indicate low $\delta^{13}\text{C}$ values of surface waters, suggest an influx of Indian Ocean thermocline waters. Recent $\delta^{13}\text{C}$ measurements along a transect south of Africa along 30°E show that the surface waters of the Agulhas Current have a carbon isotopic signature lower by $0.5\text{\textperthousand}$ than the subantarctic waters (Archambeau et al., 1998; Quentin, 1997). The important contribution of Indian Ocean waters can thus easily explain the decrease of the surface-to-bottom carbon isotopic gradient. The other peaks of low $\Delta^{13}\text{C}$ values occur independent of glacial stages (MISs 2, 3, 4, and 6) and interglacial stages (MISs 5, 7, and 13), but they correspond to the periods of maximum abundance of *G. bulloides* that are also marked by $\Delta^{18}\text{O}$ anomalies; in these cases, the $\delta^{13}\text{C}$ decrease at the surface is more likely caused by the seaward extension of ^{13}C -depleted upwelled waters.

The high $\Delta^{13}\text{C}$ values are mostly concentrated in late MIS 5 and during the 260- to 425-ka interval. As mentioned above, the high $\delta^{13}\text{C}$ values of planktonic foraminifers were interpreted as indicative of high primary productivity. These events, which interrupt the negative $\Delta^{13}\text{C}$ excursions, indicate the installation of a different regime dominated by more oligotrophic conditions.

Surface Water Gradients

The carbon isotope gradients in the surface waters are balanced by the uptake of $\Delta^{13}\text{C}$ -depleted CO_2 , resulting from surface productivity and by the inputs of $\Delta^{13}\text{C}$ -depleted CO_2 due to the vertical and lateral

F6. The $\Delta^{13}\text{C}$ gradient between *G. inflata* and *Cibicides*, *G. bulloides*, and *G. ruber* as a function of age, Hole 1087A, p. 17.



advection of nutrient-rich waters. The $\Delta^{13}\text{C}$ variations between *G. inflata* and *G. bulloides* are twice those measured between *G. inflata* and *G. ruber* (Fig. F6B, F6C); this is explained by the largest $\delta^{13}\text{C}$ variations recorded by *G. bulloides*, a species that is the most sensitive to changes in upwelling strength. The overall $\Delta^{13}\text{C}$ patterns show no correspondence with the G-IG cycles; however, these patterns document global trends toward increasing or decreasing values, which are inferred to represent major changes in the trophic regime and in the depth of the thermocline that are controlled by the lateral and vertical advective fluxes of nutrient-rich deep waters.

The minimum values of the carbon isotope gradient between *G. inflata* and *G. bulloides* are interpreted as representative of oligotrophic conditions, whereas the maximum values are indicative of mesotrophic conditions. Three steps may be identified following the evolution of the *G. inflata*-*G. bulloides* $\Delta^{13}\text{C}$ values (Fig. F6B). Starting from 500 ka, where the $\Delta^{13}\text{C}$ values are similar to the Holocene values, there is a decrease by $>1\text{\%}$ (on average) up to 400 ka; this period corresponds to the initiation of oligotrophic conditions that remain quite steady up to 350 ka. After 350 ka and up to 100 ka, this planktonic $\Delta^{13}\text{C}$ increases by $>2\text{\%}$ on average, marking the progressive development of more mesotrophic conditions. After 100 ka, the $\Delta^{13}\text{C}$ values decrease again by $\sim 1\text{\%}$ to reach the Holocene values, marking the return toward oligotrophic conditions.

The carbon isotope gradient between *G. inflata* and *G. ruber* is considered to follow the vertical movement of the thermocline: shoaling of the thermocline brings deep nutrients closer to the surface and the $\Delta^{13}\text{C}$ values decrease in the surface waters, whereas deepening of the thermocline diminishes the inputs of deep nutrients to the surface and results in the increase of $\Delta^{13}\text{C}$ values. The same three steps are also observed in the $\Delta^{13}\text{C}$ *G. inflata*-*G. ruber* record (Fig. F6C). During the period from 500 ka to 350 ka, $\Delta^{13}\text{C}$ values increase by $\sim 0.7\text{\%}$ on average, an indication for the progressive deepening of the thermocline. The second step from 350 ka to 100 ka corresponds to the progressive decrease of $\Delta^{13}\text{C}$ by $\sim 0.6\text{\%}$ and is related to the progressive shoaling of the thermocline. During the last step, $\Delta^{13}\text{C}$ increases again by $\sim 0.3\text{\%}$, suggesting that the thermocline deepened slightly to reach the present-day situation.

CONCLUSIONS

The location of Site 1087 in the Southern Cape Basin near the external boundary of the Benguela coastal upwelling system and close to the Agulhas Current retroflection regime, offers the opportunity to identify specific events in this area, such as the latitudinal and lateral migrations of the hydrographic fronts and the interconnections between the Indian and Atlantic Oceans. The oxygen and carbon isotope records of four species of planktonic and benthic foraminifers provide new information on the climatic and hydrologic changes during the last 500 k.y. in this part of the South Atlantic.

The oxygen isotope records at Site 1087 show typical G-IG cycles with a few marked differences in the global ocean signature due to the local hydrologic regime. The coldest period corresponds to MIS 12, and the warmest periods occur during MISs 5 and 11, both for surface and deep waters. The variations of the $\delta^{18}\text{O}$ gradients between surface and

deep waters are very abrupt and subjected to rapid, high-frequency oscillations; these oscillations are related to sporadic injections of Indian Ocean waters and to important and permanent modifications of the position of frontal boundaries and of the depth of the thermocline.

The carbon isotope records at Site 1087 do not follow the G-IG cycles, but they show abrupt and short-term oscillations associated with long-term trends. The variations in the $\delta^{13}\text{C}$ gradients between surface and deep waters allow us to identify an extended period of high productivity between 260 and 425 ka that is contemporary with the mid-Brunhes carbonate event. In the surface waters, the $\delta^{13}\text{C}$ gradients also display very sharp fluctuations associated with long-term trends that are controlled both by the trophic regime and by the depth of the thermocline.

ACKNOWLEDGMENTS

This study has received the financial support of the Institut National des Sciences de l'Univers of CNRS (INSU grant 98 "Géosciences Marines"). We are greatly indebted to David Hodell and an anonymous reviewer, who have substantially contributed to improve the initial manuscript.

REFERENCES

- Archambeau, A.S., Pierre, C., Poisson, A., and Schauer, B., 1998. Distributions of oxygen and carbon stable isotopes of the Southern ocean at 30°E from South Africa to Antarctica: results of the CIVA 1 cruise. *J. Mar. Syst.*, 17:25–38.
- Bassinot, F.C., Labeyrie, L.D., Vincent, E., Quidelleur, X., Shackleton, N.J., and Lancelot, Y., 1994. The astronomical theory of climate and the age of the Brunhes-Matuyama magnetic reversal. *Earth Planet. Sci. Lett.*, 126:91–108.
- Berger, W.H., Smetacek, V.S., and Wefer, G., 1989. Ocean productivity and paleoproductivity: an overview. In Berger, W.H., Smetacek, V.S., and Wefer, G. (Eds.), *Productivity of the Oceans: Present and Past*: New York (Wiley & Sons), 1–34.
- Broecker, W.S., and Henderson, G.M., 1998. The sequence of events surrounding Termination II and their implications for the cause of glacial-interglacial CO₂ changes. *Paleoceanography*, 13:352–364.
- Giraudeau, J., 1993. Planktonic foraminiferal assemblages in surface sediments from the southwest African continental margin. *Mar. Geol.*, 110:47–62.
- Giraudeau, J., and Rogers, J., 1994. Phytoplankton biomass and sea-surface temperature estimates from sea-bed distribution of nannofossils and planktonic foraminifera in the Benguela Upwelling System. *Micropaleontology*, 40:275–285.
- Hodell, D.A., 1993. Late Pleistocene paleoceanography of the South Atlantic sector of the Southern Ocean: Ocean Drilling Program Hole 704A. *Paleoceanography*, 8:47–67.
- Hodell, D.A., Charles, C.D., and Nissemann, U.S., 2000. Comparison of interglacial stages in the South Atlantic sector of the southern ocean for the past 450 kyr: implications for Marine Isotope Stage (MIS) 11. *Global Planet. Change*, 24:7–26.
- Howard, W.R., and Prell, W.L., 1994. Late Quaternary CaCO₃ production and preservation in the Southern Ocean: implications for oceanic and atmospheric carbon cycling. *Paleoceanography*, 9:453–482.
- Imbrie, J., Hays, J.D., Martinson, D.G., McIntyre, A., Mix, A.C., Morley, J.J., Pisias, N.G., Prell, W.L., and Shackleton, N.J., 1984. The orbital theory of Pleistocene climate: support from a revised chronology of the marine δ¹⁸O record. In Berger, A., Imbrie, J., Hays, J., Kukla, G., and Saltzman, B. (Eds.), *Milankovitch and Climate* (Pt. 1), NATO ASI Ser. C, Math Phys. Sci., 126:269–305.
- Jansen, J.H.F., Kuijpers, A., and Troelstra, S.R., 1986. A mid-Brunhes climatic event: long-term changes in global atmospheric and ocean circulation. *Science*, 232:619–622.
- Martinson, D.G., Pisias, N.G., Hays, J.D., Imbrie, J., Moore, T.C., Jr., and Shackleton, N.J., 1987. Age dating and the orbital theory of the ice ages: development of a high-resolution 0 to 300,000-year chronostratigraphy. *Quat. Res.*, 27:1–29.
- McManus, J.F., Oppo, D.W., and Cullen, J.L., 1999. A 0.5 million year record of millennial-scale climate variability in the North Atlantic. *Science*, 283:971–975.
- Morley, J.J., and Hays, J.D., 1979. Comparison of glacial and interglacial oceanographic conditions in the South Atlantic from variations in calcium carbonate and radiolarian distributions. *Quat. Res.*, 12:396–408.
- Pierre, C., Vangriesheim, A., and Laube-Lenfant, E., 1994. Variability of water masses and of organic production-regeneration systems as related to eutrophic, mesotrophic and oligotrophic conditions in the northeast Atlantic ocean. *J. Mar. Syst.*, 5:159–170.
- Quentin, C., 1997. Variabilité spatiale des valeurs de δ¹³C du ΣCO₂ dans l'Océan Austral superficiel: relations avec les structures hydrologiques de méso-échelle. Rapport de maîtrise Physique et Applications, UPMC, 34 pp.
- Sarnthein, M., and Tiedemann, R., 1990. Younger Dryas-Style cooling events at glacial terminations I–VI at ODP Site 658: associated benthic δ¹³C anomalies constrain meltwater hypothesis. *Paleoceanography*, 5:1041–1055.

- Shipboard Scientific Party, 1998. Site 1087. In Wefer, G., Berger, W.H., and Richter, C., et al., *Proc. ODP, Init. Repts.*, 175: College Station, TX (Ocean Drilling Program), 457–484.
- Wefer, G., Berger, W.H., Bickert, T., Donner, B., Fischer, G., Kemle-von Mücke, S., Meinecke, G., Müller, P.J., Mulitza, S., Niebler, H.-S., Pätzold, J., Schmidt, H., Schneider, R.R., and Segl, M., 1996. Late Quaternary surface circulation of the South Atlantic: the stable isotope record and implications for heat transport and productivity. In Wefer, G., Berger, W.H., Siedler, G., and Webb, D.J. (Eds.), *The South Atlantic: Present and Past Circulation*: Berlin (Springer-Verlag), 461–502.
- Winter, A., and Martin, K., 1990. Late Quaternary history of the Agulhas current. *Paleoceanography*, 5:479–486.

Figure F1. A. The $\delta^{18}\text{O}$ record of benthic foraminifer *Cibicides wuellerstorfi* as a function of depth in Hole 1075A. B. The $\delta^{18}\text{O}$ record of *C. wuellerstorfi* as a function of age in Hole 1075A. PDB = Peedee belemnite. Bold numbers 1, 5, 7, 9, 11, and 13 = marine isotope stages.

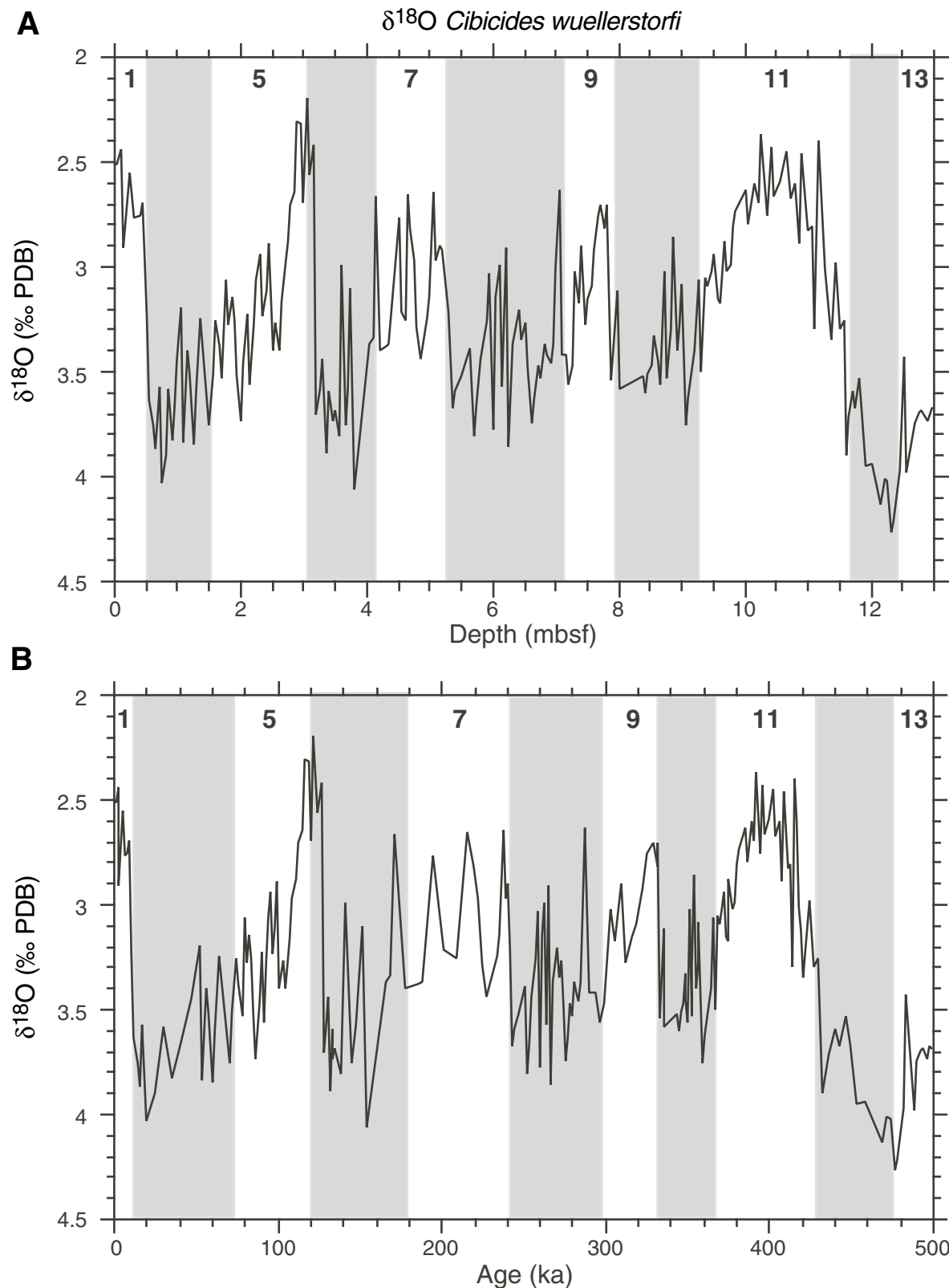


Figure F2. A. The $\delta^{18}\text{O}$ record of planktonic foraminifer *Globorotalia inflata* as a function of age in Hole 1075A. B. The $\delta^{18}\text{O}$ record of planktonic foraminifer *Globigerina bulloides* as a function of age in Hole 1075A. C. The $\delta^{18}\text{O}$ record of planktonic foraminifer *Globigerinoides ruber* as a function of age in Hole 1075A.

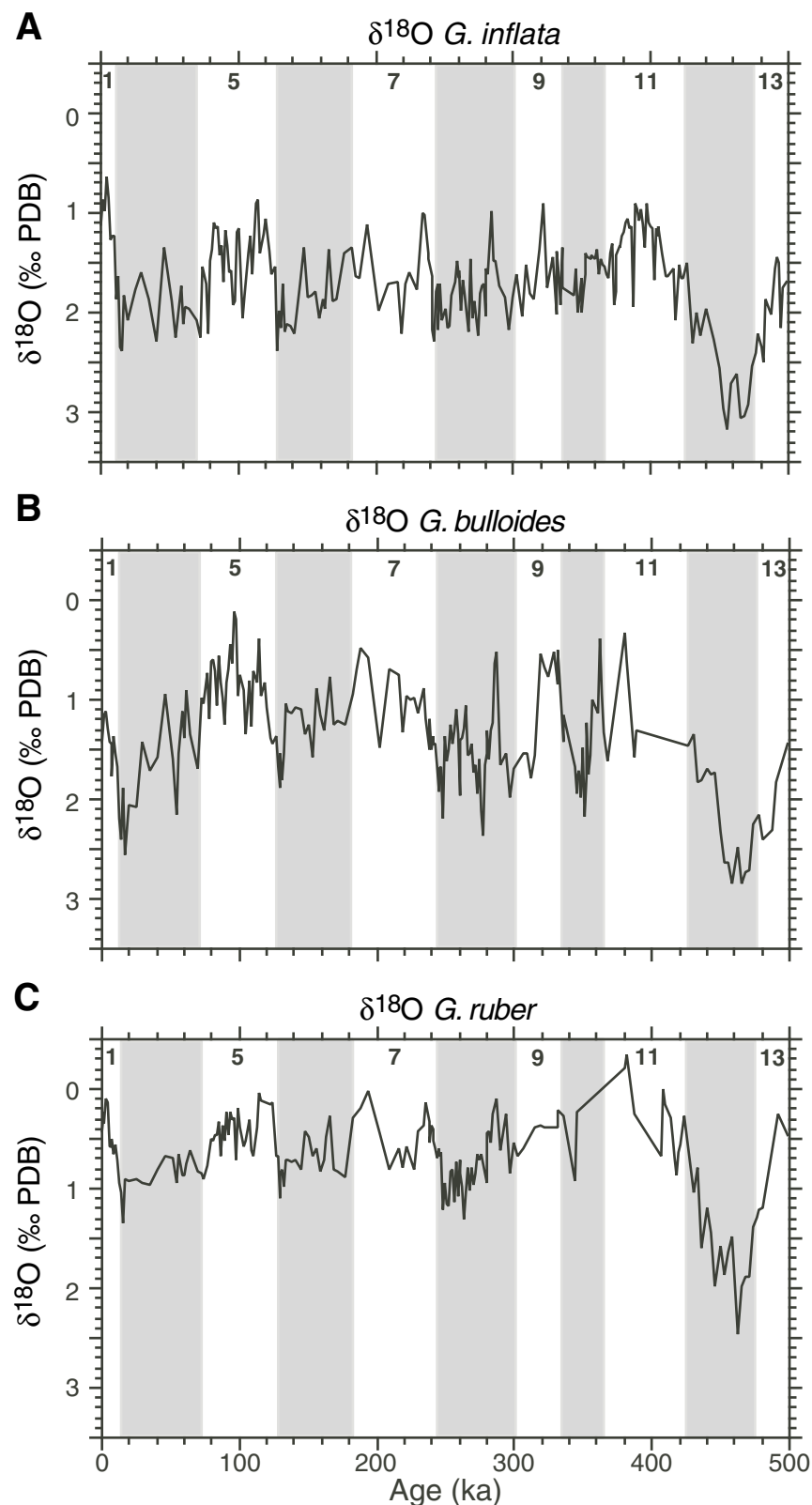


Figure F3. The $\delta^{13}\text{C}$ record of benthic foraminifer *Cibicides wuellerstorfi* as a function of age in Hole 1075A.

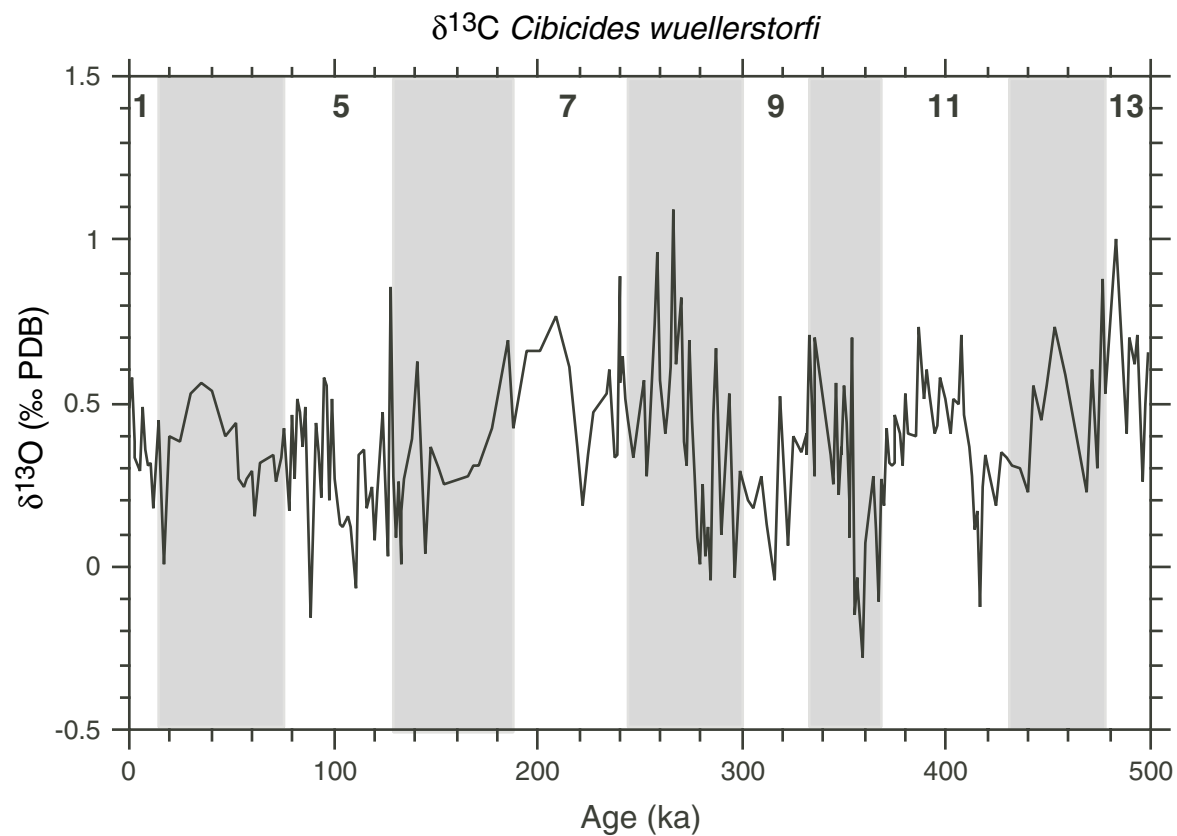


Figure F4. A. The $\delta^{13}\text{C}$ record of planktonic foraminifer *Globorotalia inflata* as a function of age in Hole 1075A. B. The $\delta^{13}\text{C}$ record of planktonic foraminifer *Globigerina bulloides* as a function of age in Hole 1075A. C. The $\delta^{13}\text{C}$ record of planktonic foraminifer *Globigerinoides ruber* as a function of age in Hole 1075A.

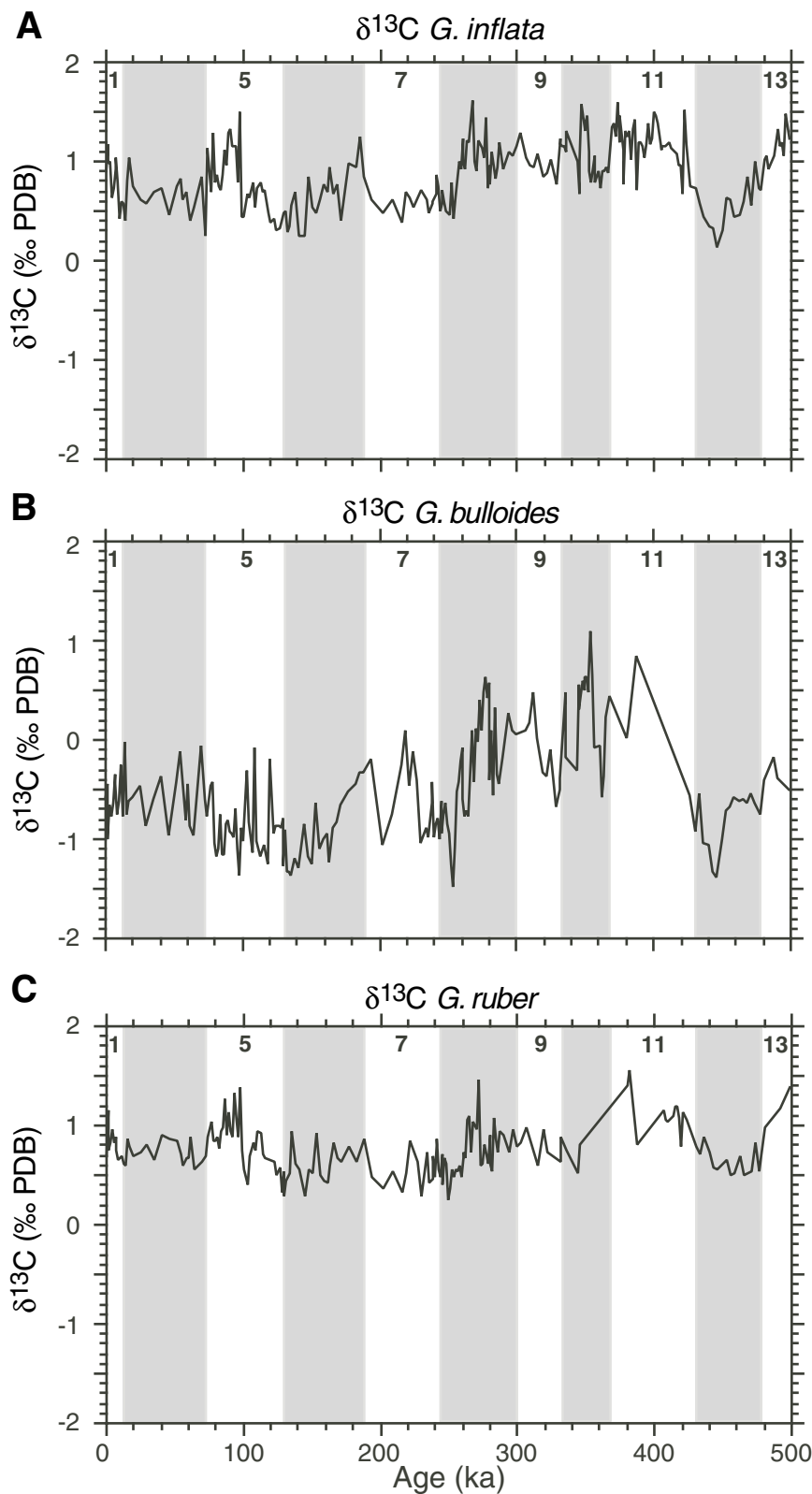


Figure F5. A. The $\Delta^{18}\text{O}$ gradient between *G. inflata* and *Cibicides* as a function of age in Hole 1087A. B. The $\Delta^{18}\text{O}$ gradient between *G. inflata* and *G. bulloides* as a function of age in Hole 1087A. C. The $\Delta^{18}\text{O}$ gradient between *G. inflata* and *G. ruber* as a function of age in Hole 1087A. The dashed lines represent the Holocene values.

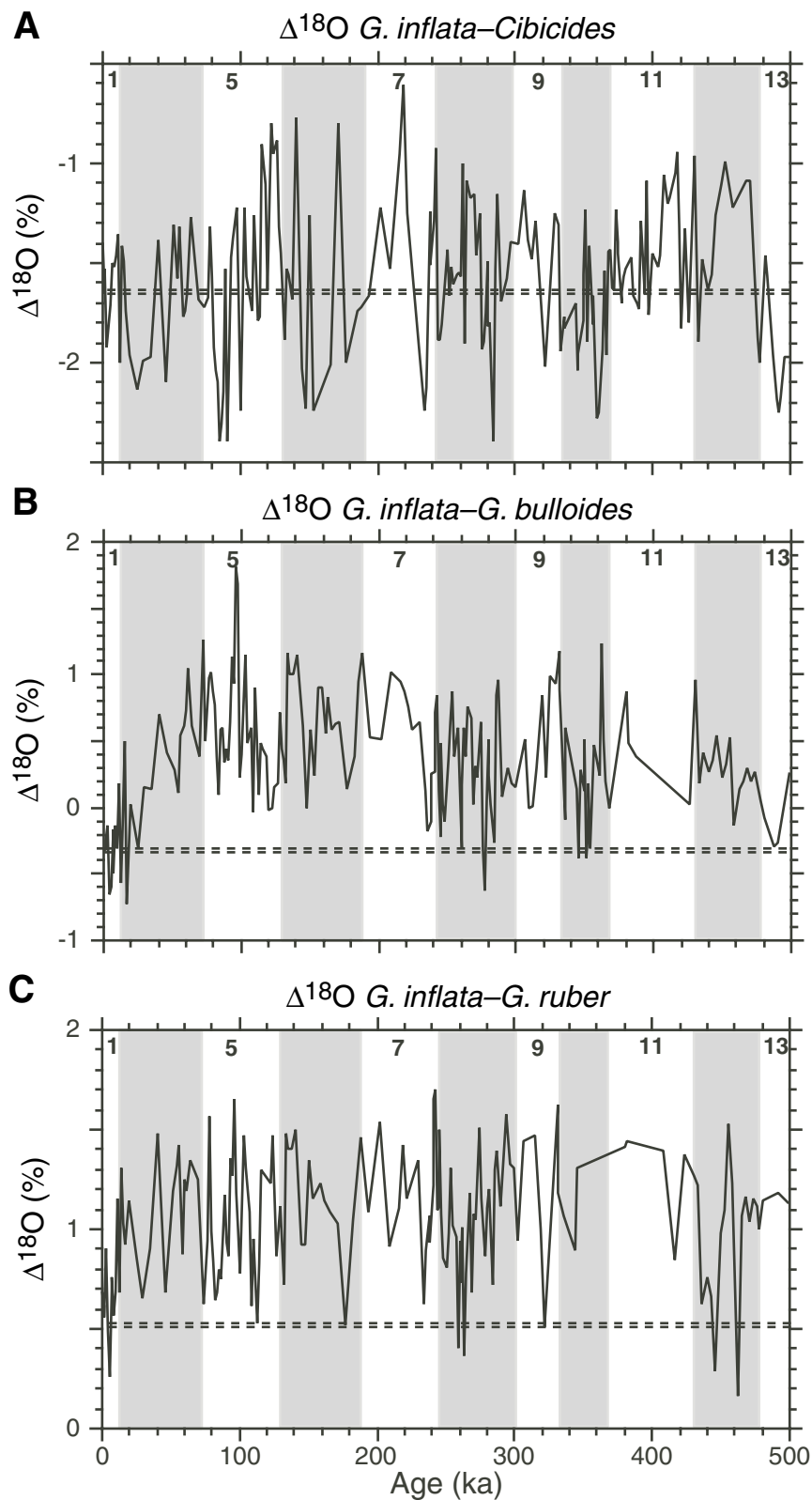


Figure F6. A. The $\Delta^{13}\text{C}$ gradient between *G. inflata* and *Cibicides* as a function of age in Hole 1087A. B. The $\Delta^{13}\text{C}$ gradient between *G. inflata* and *G. bulloides* as a function of age in Hole 1087A. C. The $\Delta^{13}\text{C}$ gradient between *G. inflata* and *G. ruber* as a function of age in Hole 1087A. The dashed lines represent the Holocene values.

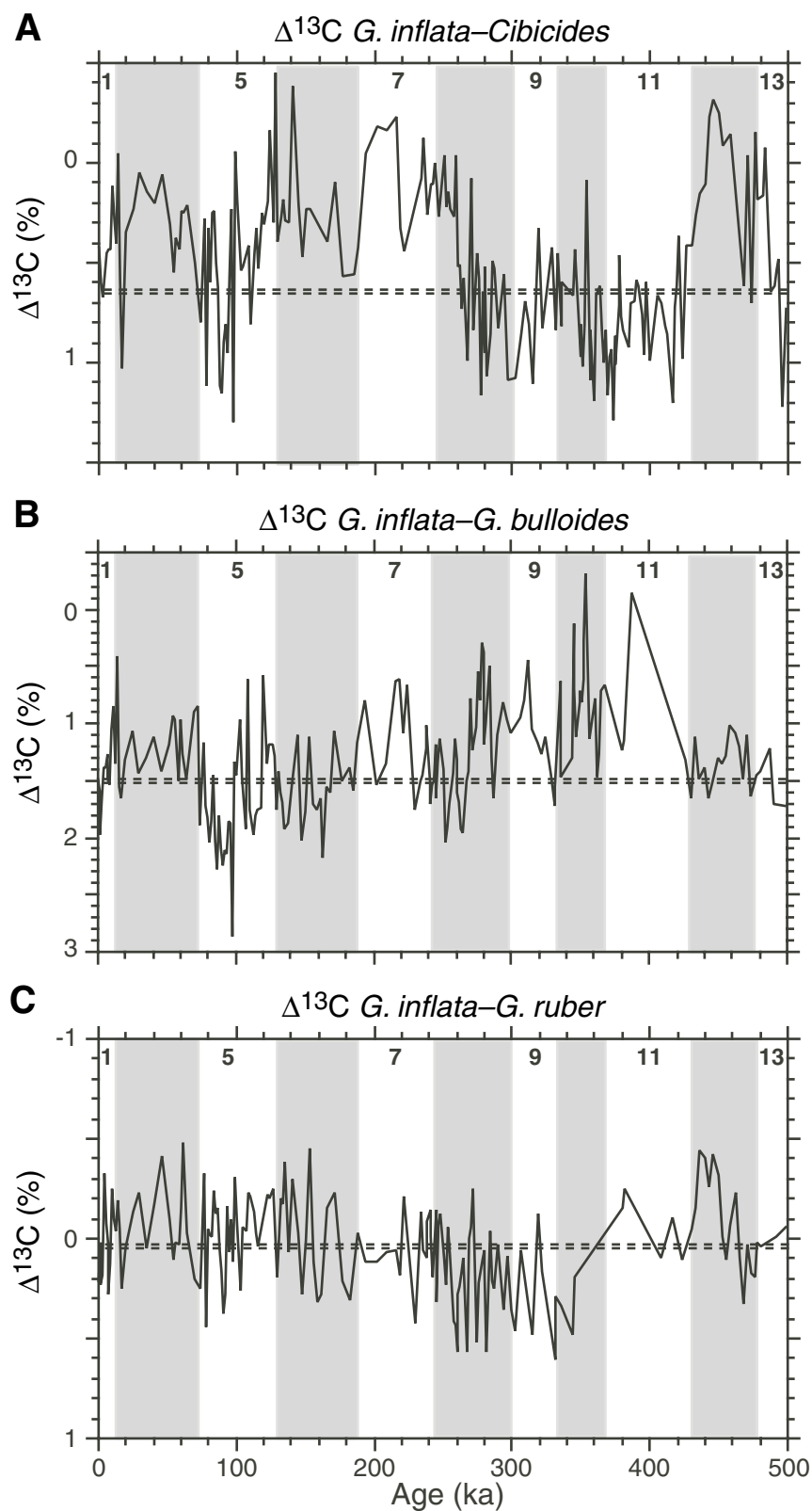


Table T1. Sample identification, depth, age, and oxygen and carbon isotopic compositions of the planktonic and benthic foraminifers, Hole 1087A.

Core, section, interval (cm)	Depth (mbsf)	Age (ka)	$\delta^{18}\text{O}$ <i>G. inflata</i>	$\delta^{13}\text{C}$ <i>G. inflata</i>	$\delta^{18}\text{O}$ <i>G. bulloides</i>	$\delta^{13}\text{C}$ <i>G. bulloides</i>	$\delta^{18}\text{O}$ <i>G. ruber</i>	$\delta^{13}\text{C}$ <i>G. ruber</i>	$\delta^{18}\text{O}$ <i>Cibicides</i>	$\delta^{13}\text{C}$ <i>Cibicides</i>
175-1087A-										
1H-1, 0-3	0.00	0	1.11	0.91	1.42	-0.58	0.43	0.70	2.51	0.49
1H-1, 5-8	0.05	1	1.07	1.03	1.18	-0.44	0.24	1.15	2.51	0.58
1H-1, 10-13	0.10	2	0.91	0.98	1.16	-1.00	0.35	0.75	2.44	0.38
1H-1, 15-18	0.15	3	0.99	1.00	1.12	-0.66	0.09	0.82	2.91	0.33
1H-1, 20-23	0.20	4	0.63	0.63	1.29	-0.76	0.14	0.96		
1H-1, 25-28	0.25	5	0.84	0.74	1.43	-0.64	0.58	0.82	2.55	0.29
1H-1, 30-33	0.30	6	1.27	0.92	1.44	-0.35	0.58	0.89	2.77	0.49
1H-1, 35-38	0.35	7	1.27	1.04	1.77	-0.45	0.51	0.76		
1H-1, 40-43	0.40	8	1.23	0.79	1.37	-0.75	0.66	0.66	2.75	0.36
1H-1, 45-48	0.45	10	1.23	0.43	1.53	-0.62	0.55	0.68	2.69	0.31
1H-1, 50-53	0.50	11	1.87	0.60	1.68	-0.25	0.72	0.70	3.23	0.32
1H-1, 55-58	0.55	12	1.63	0.58	2.19	-0.77	0.95	0.62	3.63	0.18
1H-1, 60-63	0.60	14	2.34	0.40	2.41	-0.01	1.03	0.59	3.75	0.45
1H-1, 65-68	0.65	16	2.38	0.81	1.88	-0.75	1.35	0.86	3.87	0.22
1H-1, 70-73	0.70	17	1.83	1.04	2.55	-0.62	0.91	0.79	3.57	0.01
1H-1, 75-78	0.75	19	2.07	0.75	2.05	-0.57	0.93	0.70	4.03	0.40
1H-1, 80-83	0.80	25	1.77	0.61	2.07	-0.46	0.91	0.74	3.90	0.38
1H-1, 85-88	0.85	30	1.59	0.58	1.43	-0.86	0.94	0.81	3.58	0.53
1H-1, 90-93	0.90	36	1.86	0.70	1.72	-0.60	0.96	0.65	3.83	0.56
1H-1, 95-98	0.95	41	2.28	0.74	1.58	-0.37	0.80	0.91	3.66	0.54
1H-1, 100-103	1.00	47	1.35	0.46	0.94	-0.96	0.67	0.87	3.45	0.40
1H-1, 105-108	1.05	52	1.88	0.75	1.60	-0.43	0.69	0.85	3.19	0.44
1H-1, 110-113	1.10	54	2.26	0.82	2.15	-0.11	0.94	0.71	3.84	0.27
1H-1, 115-118	1.15	56	2.08	0.62	1.54	-0.35	0.66	0.60	3.40	0.24
1H-1, 120-123	1.20	58	1.74	0.70	1.12	-0.80	0.86	0.67	3.51	0.27
1H-1, 125-128	1.25	60	2.11	0.53	1.38	-0.44	0.86	0.68	3.85	0.29
1H-1, 130-133	1.30	62	1.95	0.40	0.90	-0.87	0.76	0.88	3.60	0.15
1H-1, 135-138	1.35	64	1.97	0.53	1.35	-0.96	0.62	0.56	3.24	0.32
1H-2, 0-3	1.50	70	2.07	0.84	1.69	-0.05	0.82	0.64	3.75	0.34
1H-2, 5-8	1.55	72	1.73	0.47	0.98	-0.59	0.85	0.70	3.51	0.26
1H-2, 10-13	1.60	74	1.53	1.13	1.03	-0.76	0.90	0.88	3.25	0.33
1H-2, 15-18	1.65	76	1.71	0.70	0.74	-0.46	0.77	1.03	3.38	0.42
1H-2, 20-23	1.70	78	2.21	1.29	1.19	-0.43	0.64	0.85	3.53	0.17
1H-2, 25-28	1.75	80	1.49	0.79	0.62	-1.04	0.50	0.84	3.06	0.46
1H-2, 30-33	1.80	81	1.36	0.87	0.59	-1.17	0.52	0.89	3.28	0.27
1H-2, 35-38	1.85	83	1.10	0.76	0.71	-1.10	0.46	0.77	3.14	0.51
1H-2, 40-43	1.90	84	1.15	0.71	1.06	-0.75	0.47	0.95	3.25	0.47
1H-2, 45-48	1.95	85	1.13	0.87	0.55	-1.15	0.33	0.99	3.52	0.37
1H-2, 50-53	2.00	87	1.42	1.12	0.82	-1.16	0.67	1.27	3.73	0.49
1H-2, 55-58	2.05	88	1.32	0.96	0.98	-0.84	0.37	0.91	3.46	-0.16
1H-2, 60-63	2.10	90	1.69	1.29	1.25	-0.80	0.52	1.13	3.22	0.14
1H-2, 65-68	2.15	91	1.17	1.33	0.82	-0.92	0.24	0.95	3.56	0.44
1H-2, 70-73	2.20	92	1.33	1.16	0.69	-0.95	0.46	0.88	3.28	0.35
1H-2, 75-78	2.25	94	1.59	1.16	0.45	-0.98	0.23	1.32	3.06	0.21
1H-2, 80-83	2.30	95	1.57	1.15	0.64	-0.70	0.30	1.08	2.94	0.58
1H-2, 85-88	2.35	96	1.93	0.78	0.11	-1.09	0.28	0.88	3.23	0.55
1H-2, 90-93	2.40	98	1.89	1.50	0.20	-1.37	0.71	1.38	3.11	0.20
1H-2, 95-98	2.45	99	1.19	0.45	0.96	-0.88	0.20	0.76	2.89	0.51
1H-2, 100-103	2.50	101	1.16	0.45	0.76	-1.01	0.38	0.55	3.40	0.27
1H-2, 115-118	2.65	107	1.40	0.79	0.80	-1.14	0.31	0.83	3.16	0.15
1H-2, 125-128	2.75	111	1.62	0.74	0.72	-1.02	0.67	0.95	2.88	-0.07
1H-2, 130-133	2.80	112	0.91	0.79	0.82	-1.18	0.38	0.92	2.70	0.34
1H-2, 135-138	2.85	114	0.87	0.69	0.39	-1.11	0.04	0.72	2.64	0.36
1H-2, 140-143	2.90	116	1.41	0.71	0.96	-1.05	0.11	0.67	2.31	0.18
1H-2, 145-148	2.95	118	1.21	0.49	0.82	-1.25			2.32	0.24
1H-3, 0-3	3.00	120	1.06	0.39	1.08	-0.19	0.25	0.79	2.69	0.08
1H-3, 5-8	3.05	122	1.39	0.42	1.39	-0.94	0.16	0.64	2.19	0.23
1H-3, 10-13	3.10	124	1.61	0.31	1.45	-0.87	0.14	0.51	2.56	0.47
1H-3, 15-18	3.15	126	1.54	0.33	1.36	-0.86	0.67	0.58	2.42	0.03
1H-3, 20-23	3.20	128	2.38	0.41	1.67	-0.88	0.67	0.32	3.70	0.86
1H-3, 25-28	3.25	129	2.07	0.45	1.89	-0.78	1.09	0.53	3.58	0.28
1H-3, 30-33	3.30	130	2.10	0.54	1.54	-1.27	0.87	0.29	3.44	0.09
1H-3, 35-38	3.35	131	2.16	0.51	1.81	-0.91	0.81	0.45	3.89	0.26
1H-3, 40-43	3.40	133	1.71	0.28	1.53	-1.33	0.99	0.48	3.59	0.01
1H-3, 45-48	3.45	134	2.20	0.35	1.03	-1.33	0.72	0.52	3.73	0.17
1H-3, 50-53	3.50	135	2.12	0.56	1.11	-1.37	0.72	0.94	3.68	0.27
1H-3, 55-58	3.55	138	2.13	0.69	1.13	-1.19	0.73	0.62	3.81	0.39

Table T1 (continued).

Core, section, interval (cm)	Depth (mbsf)	Age (ka)	$\delta^{18}\text{O}$ <i>G. inflata</i>	$\delta^{13}\text{C}$ <i>G. inflata</i>	$\delta^{18}\text{O}$ <i>G. bulloides</i>	$\delta^{13}\text{C}$ <i>G. bulloides</i>	$\delta^{18}\text{O}$ <i>G. ruber</i>	$\delta^{13}\text{C}$ <i>G. ruber</i>	$\delta^{18}\text{O}$ <i>Cibicides</i>	$\delta^{13}\text{C}$ <i>Cibicides</i>
1H-3, 60-63	3.60	141	2.22	0.25	1.07	-1.28	0.72	0.55	2.99	0.63
1H-3, 65-68	3.65	145	1.72	0.25	1.10	-0.85	0.80	0.28	3.75	0.04
1H-3, 70-73	3.70	148	1.34	0.84	1.35	-1.18	0.42	0.56	3.57	0.37
1H-3, 75-78	3.75	151	1.84	0.53	1.26	-1.25	0.49	0.52	3.10	0.30
1H-3, 80-83	3.80	154	1.82	0.48	1.58	-0.64	0.67	0.93	4.06	0.25
1H-3, 85-88	3.85	156	1.79	0.62	0.89	-1.09	0.60	0.50		
1H-3, 90-93	3.90	159	2.05	0.77	1.15	-0.99	0.82	0.45		
1H-3, 95-98	3.95	161	1.86	0.70	1.30	-0.95	0.72	0.42		
1H-3, 100-103	4.00	164	1.53	0.44	1.14	-1.23	0.49	0.60		
1H-3, 105-108	4.05	166	1.36	0.67	0.77	-0.89	0.27	0.82	3.37	0.28
1H-3, 110-113	4.10	169	1.89	0.77	1.26	-0.83	0.80	0.68	3.34	0.31
1H-3, 115-118	4.15	171	1.86	0.41	1.22	-0.66	0.83	0.64	2.66	0.31
1H-3, 120-123	4.20	177	1.40	0.99	1.26	-0.52	0.88	0.78	3.40	0.42
1H-3, 125-128	4.25	183	1.34	0.95	0.95	-0.44	0.29	0.64		
1H-3, 130-133	4.30	185	1.64	1.25	0.69	-0.33			3.38	0.69
1H-3, 135-138	4.35	187	1.65	0.84	0.48	-0.33	0.19	0.87	3.37	0.42
1H-4, 0-3	4.50	194	1.11	0.61	0.58	-0.19	0.02	0.49	2.77	0.66
1H-4, 5-8	4.55	201	1.99	0.48	1.48	-1.06	0.45	0.36	3.21	0.66
1H-4, 10-13	4.60	209	1.72	0.61	0.70	-0.74	0.81	0.54	3.25	0.77
1H-4, 15-18	4.65	216	1.70	0.38	0.75	-0.24	0.59	0.32	2.65	0.61
1H-4, 20-23	4.70	219	2.21	0.70	1.33	0.09	0.79	0.52	2.82	0.37
1H-4, 25-28	4.75	222	1.72	0.63	0.96	-0.46	0.57	0.84	2.97	0.19
1H-4, 30-33	4.80	224	1.59	0.54	1.01	-0.12			3.29	0.34
1H-4, 35-38	4.85	227	1.60	0.60	0.99	-0.41	0.80	0.63	3.44	0.47
1H-4, 40-43	4.90	230	1.53	0.61	1.13	-1.04	0.42	0.29		
1H-4, 47-49	4.97	234	1.00	0.61	0.88	-0.89	0.37	0.74	3.24	0.53
1H-4, 50-53	5.00	235	1.02	0.48	1.20	-0.98	0.13	0.42	3.14	0.60
1H-4, 55-58	5.05	238	1.40	0.57	1.50	-0.64	0.33	0.47	2.64	0.33
1H-4, 60-63	5.10	239	1.46	0.60	1.20	-0.42	0.53	0.69	2.97	0.34
1H-4, 65-68	5.15	240	1.41	0.42	1.51	-0.98	0.36	0.49	2.90	0.89
1H-4, 70-73	5.20	240	1.63	0.67	1.36	-0.85	0.41	0.81	2.92	0.56
1H-4, 75-78	5.25	241	2.17	0.86	1.45	-0.85	0.52	0.87	3.49	0.43
1H-4, 80-83	5.30	242	2.29	0.75	1.45	-0.79	0.59	0.56	3.21	0.64
1H-4, 85-88	5.35	243	1.79	0.51	1.67	-0.99	0.69	0.49	3.67	0.51
1H-4, 90-93	5.40	245	1.71	0.57	1.93	-0.61	0.59	0.71	3.59	0.45
1H-4, 95-98	5.45	246	2.17	0.72	1.69	-0.94	0.67	0.40		
1H-4, 105-108	5.55	248	2.08	0.50	2.19	-0.64	1.22	0.62		
1H-4, 110-113	5.60	250	1.61	0.38	1.36	-0.84	0.95	0.26		
1H-4, 115-118	5.65	251	1.96	0.47	1.61	-0.94	1.15	0.37	3.39	0.51
1H-4, 120-123	5.70	252	2.15	0.79	1.50	-1.25	1.17	0.56	3.81	0.57
1H-4, 126-128	5.75	254	2.14	0.42	1.26	-1.48	0.83	0.48	3.66	0.28
1H-4, 130-133	5.80	255	1.83	0.64	1.45	-1.07	0.81	0.56	3.44	0.41
1H-4, 135-138	5.85	256	2.12	0.96	1.30	-0.52	1.13	0.54		
1H-4, 140-143	5.90	257	1.69	1.01	1.09	-0.42	0.73	0.60	3.25	0.74
1H-4, 145-148	5.95	259	1.48	0.92	1.34	-0.22	1.08	0.49	3.03	0.96
1H-5, 0-3	6.00	260	1.65	1.24	1.96	-0.07	0.71	0.67	3.78	0.57
1H-5, 5-8	6.05	261	1.57	1.01	1.40	-0.60	0.84	0.73	3.14	0.49
1H-5, 10-13	6.10	262	1.99	0.92	1.39	-0.77	0.98	0.68	2.99	0.41
1H-5, 15-18	6.15	264	1.67	1.22	1.29	-0.71	1.30	1.05	3.57	0.49
1H-5, 20-23	6.20	265	1.82	1.19	1.06	-0.76	1.04	1.09	2.91	0.61
1H-5, 25-28	6.25	266	1.96	0.87	1.56	-0.35	0.79	0.74	3.86	1.09
1H-5, 30-33	6.30	268	2.20	1.61	1.53	0.10	1.02	1.04	3.37	0.62
1H-5, 35-38	6.35	269	1.47	1.00	1.45	-0.42	0.79	1.00		
1H-5, 40-43	6.40	270	2.05	0.90	1.74	0.12	0.97	0.96	3.20	0.82
1H-5, 45-48	6.45	271	1.89	1.22	1.66	-0.01	0.84	1.47	3.35	0.38
1H-5, 51-53	6.51	273	2.16	0.79	1.94	0.40	0.65	0.60	3.27	0.31
1H-5, 56-58	6.56	274	2.23	1.14	1.59	0.10	0.72	0.62	3.48	0.69
1H-5, 61-63	6.61	275	1.81	1.03	2.11	0.48	0.66	0.81	3.74	0.45
1H-5, 66-68	6.66	277	1.74	1.44	2.37	0.64			3.63	0.28
1H-5, 71-73	6.71	278	1.72	0.73	1.66	0.43	0.85	0.62	3.47	0.09
1H-5, 76-78	6.76	279	2.04	0.96	1.53	0.58	0.94	0.90	3.53	0.01
1H-5, 81-83	6.81	281	1.55	0.77	1.31	-0.41	0.44	0.62	3.37	0.25
1H-5, 86-88	6.86	282	1.62	1.1	1.59	0.1	0.42	0.53	3.42	0.03
1H-5, 91-93	6.91	283	1.60	0.76	1.31	-0.56	0.54	1.07	3.46	0.12
1H-5, 96-98	6.96	284	0.98	0.82	1.24	0.33	0.26	0.86	3.37	-0.04
1H-5, 100-102	7.00	285	1.48	0.95	0.64	-0.35	0.18	0.74	3.01	0.46
1H-5, 106-108	7.06	287	1.48	1.20	0.52	-0.45	0.09	0.95	2.63	0.67
1H-5, 111-113	7.11	290	1.73	0.93	1.65	-0.17	0.61	0.90	3.42	0.10
1H-5, 116-118	7.16	293	1.84	1.09	1.54	0.27	0.26	0.73	3.42	0.53

Table T1 (continued).

Core, section, interval (cm)	Depth (mbsf)	Age (ka)	$\delta^{18}\text{O}$ <i>G. inflata</i>	$\delta^{13}\text{C}$ <i>G. inflata</i>	$\delta^{18}\text{O}$ <i>G. bulloides</i>	$\delta^{13}\text{C}$ <i>G. bulloides</i>	$\delta^{18}\text{O}$ <i>G. ruber</i>	$\delta^{13}\text{C}$ <i>G. ruber</i>	$\delta^{18}\text{O}$ <i>Cibicides</i>	$\delta^{13}\text{C}$ <i>Cibicides</i>
1H-5, 121-123	7.21	296	2.17	1.06	1.99	0.10	0.84	0.97	3.56	-0.03
1H-5, 126-128	7.26	300	1.85	1.15	1.70	0.06	0.54	0.79	3.47	0.29
1H-5, 131-133	7.31	303	1.62	1.28			0.68	0.82	3.02	0.20
1H-5, 136-138	7.36	306	2.04	1.04	1.53	0.09	0.60	0.98	3.17	0.18
1H-5, 141-143	7.41	309	1.52	0.97	1.53	0.18			2.9	0.28
1H-5, 146-148	7.46	312	1.80	0.94	1.79	0.49			3.28	0.13
1H-6, 1-3	7.51	315	1.86	1.07	1.56	0.02	0.39	0.59	3.15	-0.04
1H-6, 6-8	7.56	319	1.37	0.85	0.53	-0.32	0.37	0.97	3.09	0.52
1H-6, 11-13	7.61	322	0.90	0.89	0.67	-0.37	0.39	0.73	2.92	0.06
1H-6, 16-18	7.66	325	1.26	0.80	0.77	-0.10			2.75	0.40
1H-6, 21-23	7.71	328	1.45	0.77	0.52	-0.68			2.70	0.35
1H-6, 26-28	7.76	331	2.02	1.24	0.84	-0.49	0.39	0.63	2.82	0.41
1H-6, 31-33	7.81	332	1.39	1.18	0.50	-0.38	0.21	0.89	2.70	0.34
1H-6, 36-38	7.86	333	1.60	1.16					3.54	0.71
1H-6, 41-43	7.91	334	1.93	1.16						
1H-6, 47-49	7.97	335	1.34	1.10	1.43	0.48	0.27	0.76	3.11	0.28
1H-6, 51-53	8.01	336	1.75	1.30	1.15	-0.17			3.58	0.70
2H-1, 20-22	8.40	344	1.82	1.00	1.68	-0.30	0.93	0.52	3.52	0.34
2H-1, 23-26	8.43	345	1.56	0.68	1.94	0.55			3.60	0.25
2H-1, 26-28	8.46	346	1.55	1.00	1.81	0.31	0.24	0.81	3.51	0.56
2H-1, 36-38	8.56	348	2.32	1.28	1.98	0.59			3.33	0.37
2H-1, 41-43	8.61	349	1.66	1.31	1.54	0.50			3.45	0.34
2H-1, 46-48	8.66	350	2.00	1.36	1.48	0.64			3.56	0.55
2H-1, 51-53	8.71	351	1.79	1.46	2.17	0.64			3.02	0.44
2H-1, 56-58	8.76	352	1.61	1.10	1.77	0.49			3.53	0.20
2H-1, 61-63	8.81	353	1.41	0.90	1.23	0.62			3.30	0.09
2H-1, 66-68	8.86	354	1.45	0.79	1.75	1.10			2.86	0.70
2H-1, 71-73	8.91	355	1.50	0.86	1.56	0.66			3.40	-0.15
2H-1, 76-78	8.96	356	1.47	1.06	1.00	-0.08			3.28	-0.03
2H-1, 81-83	9.01	357	1.42	0.79					3.08	-0.05
2H-1, 86-88	9.06	359	1.47	0.91					3.75	-0.28
2H-1, 91-93	9.11	361	1.37	0.73	1.13	-0.05			3.62	0.07
2H-1, 96-98	9.16	362	1.62	0.90	0.39	-0.57				
2H-1, 101-103	9.21	364	1.47	0.90	0.95	-0.37			3.40	0.28
2H-1, 106-108	9.26	365	1.52	0.95	1.32	0.24			3.06	0.11
2H-1, 111-113	9.31	366	1.54	0.89					3.50	-0.11
2H-1, 116-118	9.36	368	1.61	1.11	1.62	0.44			3.05	0.27
2H-1, 121-123	9.41	369	1.66	1.35					3.09	0.19
2H-1, 126-128	9.46	370	1.4	1.39					3.02	0.42
2H-1, 131-133	9.51	372	1.31	1.25					2.94	0.32
2H-1, 136-138	9.56	373	1.92	1.6					3.15	0.31
2H-1, 141-143	9.61	374	1.78	1.19					3.17	0.32
2H-1, 146-148	9.66	375	1.43	1.47					2.88	0.46
2H-2, 0-3	9.70	377	1.32	1.12					3.02	0.41
2H-2, 6-8	9.76	378	1.35	0.77					2.99	0.31
2H-2, 11-13	9.81	380	1.24	1.30					2.81	0.53
2H-2, 16-18	9.86	381	1.20	1.25	0.32	0.02	-0.21	1.40	2.73	0.41
2H-2, 21-23	9.91	382	1.10	1.30	0.62	0.15	-0.34	1.55		
2H-2, 25-27	9.95	383	1.05	1.02					3.16	0.39
2H-2, 31-33	10.01	385	1.16	1.32					2.63	0.40
2H-2, 36-38	10.06	386	1.14	1.43					2.80	0.73
2H-2, 40-43	10.10	387	1.95	0.71	1.57	0.85	0.25	0.80	2.50	0.55
2H-2, 45-48	10.15	389	0.90	1.20	1.3	-1.26			2.60	0.51
2H-2, 51-53	10.21	390	0.96	1.19					2.69	0.6
2H-2, 56-58	10.26	391	1.08	1.15					2.37	0.53
2H-2, 61-64	10.31	393	0.97	1.03						
2H-2, 66-68	10.36	394	1.11	1.17					2.76	0.41
2H-2, 71-73	10.41	395	1.34	1.39					2.43	0.43
2H-2, 76-78	10.46	397	0.90	1.18					2.66	0.58
2H-2, 81-83	10.51	398	1.10	1.24					2.19	0.77
2H-2, 86-88	10.56	400	1.14	1.50					2.59	0.51
2H-2, 92-94	10.62	401	1.16	1.46					2.70	0.53
2H-2, 96-98	10.66	402	1.12	1.10					2.45	0.41
2H-2, 101-103	10.71	403	1.15	1.25					2.67	0.51
2H-2, 106-108	10.76	405	1.23	1.11					2.49	0.75
2H-2, 111-113	10.81	406	1.14	1.16					2.60	0.50
2H-2, 116-118	10.86	407	1.91	0.80	2.33	-0.22	0.67	1.15	2.89	0.71
2H-2, 121-123	10.91	409	1.58	1.21			0.01	1.06	2.46	0.46
2H-2, 126-128	10.96	410					0.15	1.03	2.51	0.54

Table T1 (continued).

Core, section, interval (cm)	Depth (mbsf)	Age (ka)	$\delta^{18}\text{O}$ <i>G. inflata</i>	$\delta^{13}\text{C}$ <i>G. inflata</i>	$\delta^{18}\text{O}$ <i>G. bulloides</i>	$\delta^{13}\text{C}$ <i>G. bulloides</i>	$\delta^{18}\text{O}$ <i>G. ruber</i>	$\delta^{13}\text{C}$ <i>G. ruber</i>	$\delta^{18}\text{O}$ <i>Cibicides</i>	$\delta^{13}\text{C}$ <i>Cibicides</i>
2H-2, 131-133	11.01	411	1.63	1.19					2.83	0.37
2H-2, 136-138	11.06	413	1.64	1.14					2.81	0.28
2H-2, 141-143	11.11	414	1.57	0.89			0.28	1.09	3.30	0.11
2H-2, 146-148	11.16	415	1.35	1.04			0.49	1.19	2.40	0.17
2H-3, 6-8	11.26	418	2.07	0.96			0.87	1.07	3.01	0.24
2H-3, 11-13	11.31	419	1.81	0.96			0.64	0.79	3.12	0.34
2H-3, 16-18	11.36	420	1.52	0.67			0.55	1.13	3.35	0.30
2H-3, 20-23	11.40	422	1.65	1.52						
2H-3, 25-27	11.45	424	1.65	1.17			0.27	1.06	2.98	0.19
2H-3, 31-33	11.51	427	1.50	0.76	1.47	-0.56			3.30	0.35
2H-3, 36-38	11.56	430	2.30	0.74	1.34	-0.92	1.03	0.79	3.26	0.33
2H-3, 41-43	11.61	433	2.01	0.57	1.82	-0.54	0.79	0.72	3.90	0.31
2H-3, 45-47	11.65	436	2.23	0.45	1.81	-1.04	1.60	0.89	3.71	0.30
2H-3, 51-53	11.71	440	1.96	0.34	1.69	-1.05	1.20	0.74	3.59	0.23
2H-3, 56-58	11.76	443	2.11	0.32	1.76	-1.33	1.45	0.58	3.67	0.55
2H-3, 61-63	11.81	446	2.27	0.13	1.73	-1.39	1.98	0.55	3.53	0.45
2H-3, 66-68	11.86	449	2.55	0.30	2.33	-1.00	1.57	0.62	3.66	0.55
2H-3, 71-73	11.91	452	2.96	0.64	2.63	-0.71	1.86	0.65	3.95	0.73
2H-3, 76-78	11.96	455	3.17	0.61	2.64	-0.67	1.64	0.50	3.73	0.65
2H-3, 80-82	12.00	459	2.72	0.45	2.85	-0.57	1.49	0.52	3.94	0.59
2H-3, 86-88	12.06	462	2.62	0.47	2.48	-0.62	2.46	0.70	4.09	0.54
2H-3, 91-93	12.11	465	3.05	0.60	2.85	-0.60	1.98	0.50		
2H-3, 96-98	12.16	468	3.04	0.85	2.74	-0.64	1.88	0.52	4.13	0.23
2H-3, 101-103	12.21	471	2.92	0.56	2.72	-0.54	1.88	0.53	4.01	0.60
2H-3, 106-108	12.26	474	2.53	1.00	2.26	-0.64	1.38	0.83	4.02	0.30
2H-3, 111-113	12.31	476	2.40	0.73			1.28	0.54	4.27	0.88
2H-3, 116-118	12.36	478	2.21	0.71	2.15	-0.75	1.21	0.69	4.21	0.53
2H-3, 120-122	12.40	480	2.34	1.02	2.41	-0.40	1.20	0.98		
2H-3, 126-128	12.46	482	2.51	1.05					3.97	0.89
2H-3, 131-133	12.51	483	1.86	0.92					3.43	1.00
2H-3, 136-138	12.56	488	2.02	1.05	2.31	-0.17			3.98	0.41
2H-4, 0-2	12.70	490	1.56	1.32	1.83	-0.39			3.74	0.70
2H-4, 6-8	12.76	492	1.44	1.16			0.26	1.17	3.69	0.62
2H-4, 11-13	12.81	493	1.51	1.19					3.68	0.71
2H-4, 16-18	12.86	495	2.15	1.05						
2H-4, 20-22	12.90	496	1.76	1.48					3.73	0.26
2H-4, 25-27	12.95	498	1.70	1.23	1.44	-0.49			3.67	0.50
2H-4, 30-32	13.00	500	1.65	1.36	1.64	-0.31	0.52	1.44	3.70	0.81

Table T2. Age-control points used for the age extrapolation, Hole 1087A.

Depth (mbsf)	Age (ka)	Isotopic event
0.52	11	2.0
0.75	19	2.2
1.05	52	3.3
1.75	80	5.1
2.45	99	5.3
3.05	122	5.5
3.17	127	6.0
3.50	135	6.2
3.75	151	6.4
4.15	171	6.5
4.25	183	6.6
4.50	194	7.1
4.65	216	7.3
5.05	238	7.5
5.30	242	8.0
7.06	287	8.5
7.41	309	9.1
7.75	331	9.3
9.06	357	10.4
9.20	362	11.0
11.50	423	12.0
12.00	434	12.2
12.25	471	12.4
12.40	478	13.0
14.20	538	14.0
15.00	574	15.0